Analytical Solutions to the Stochastic Kinetic Equation for Liquid and Ice Particle Size Spectra. Part I: Small-size fraction

Vitaly I. Khvorostyanov

Central Aerological Observatory, Dolgoprudny, Moscow Region, Russian Federation

Judith A. Curry

School of Earth and Atmospheric Sciences, Georgia Institute of Technology, Atlanta, Georgia

(Manuscript received XX Month 2007, in final form XX Month 2007)

Corresponding author address:

Dr. J. A. Curry
School of Earth and Atmospheric Sciences
Georgia Institute of Technology
Phone: (404) 894-3948
Fax: (404) 894-5638
curryja@eas.gatech.edu

Abstract

The kinetic equation of stochastic condensation for cloud drop size spectra is extended to account for crystalline clouds and also to include the accretion/aggregation process. The size spectra are separated into small and large size fractions that correspond to cloud drops (ice) and rain (snow). In Part I, we derive analytical solutions for the small-size fraction of the spectra that correspond to cloud drops and cloud ice particles that can be identified with cloud liquid water or cloud ice water content used in bulk microphysical schemes employed in cloud and climate models. Solutions for the small-size fraction have the form of generalized gamma distributions. Simple analytical expressions are found for parameters of the gamma distributions that are functions of quantities that are available in cloud and climate models: liquid or ice water content and its vertical gradient, mean particle radius or concentration, and supersaturation or vertical velocities. Equations for the gamma distribution parameters provide an explanation of the dependence of observed spectra on atmospheric dynamics, cloud temperature, and cloud liquid water or ice water content. The results are illustrated with example calculations for a crystalline cloud. The analytical solutions and expressions for the parameters presented here can be used for parameterization of the small-size fraction size spectra in liquid and crystalline clouds and related quantities (e.g., optical properties, lidar and radar reflectivities).

1. Introduction

Parameterization of cloud microphysics in a bulk cloud model or general circulation model (GCM) is usually based on the use of some *a priori* prescribed analytical functions that describe the shape of the drop or crystal size spectra. Such functions are typically selected from known empirical fits to the observed size spectra. Thorough reviews of these parameterizations and the experimental data on which they are based are given by Cotton and Anthes (1989), Young (1993), and Pruppacher and Klett (1997, hereafter PK97).

Generalized gamma distributions have been found to provide a reasonable approximation for cloud and fog drops with modal radii of a few microns (e.g., Levin 1954; Dyachenko 1959; PK97)

$$f(r) = c_N r^p \exp(-\beta r^\lambda) . \tag{1.1}$$

Here, $p > 0$ is the spectral index or the shape parameter of the spectrum, β and λ determine its exponential tail, and c_N is a normalization constant. It is often assumed that $\lambda = 1$,

$$f(r) = c_N r^p \exp(-\beta r) , \tag{1.2}$$

which is referred to as a simple gamma distribution.

The index p determines the relative spectral dispersion σ_r of the gamma distribution (1.2)

$$\sigma_r = \frac{1}{N\bar{r}} \left(\int_0^\infty (r - \bar{r})^2 f(r) dr \right)^{1/2} = (p+1)^{-1/2} , \tag{1.3}$$

Typical values for liquid clouds of p = 6 - 15 were measured by Levin (1954) and confirmed in many subsequent experiments (e.g. PK97). These values of p correspond to values of the relative dispersion σ_r = 0.38 - 0.25.

It was found that the inverse power law,

$$f(r) = c_N r^p , \qquad p < 0 , \tag{1.4}$$

can approximate the spectrum of larger drops in some liquid clouds in the radius range from 100 to between 300 and 800 μm with p = -2 to - 12 (Okita 1961; Borovikov et al. 1965; Nevzorov

1967; Ludwig and Robinson 1970). The expression (1.4) has also been used to represent ice crystal size spectra in cirrus and frontal clouds in the intermediate size region from ~20 to between 100 and 800 μm, with values of p in the range -2 to -8 (e.g. Heymsfield and Platt 1984, hereafter HP84; Platt 1997; Poellot et al. 1999; Ryan 2000). Note that (1.4) is a particular case of the gamma distribution (1.2) with $\beta = 0$.

These empirical spectra are widely used in the remote sensing of clouds (e.g., Ackerman and Stephens 1987; Matrosov et al., 1994; Sassen and Liao 1996; Platt 1997) and also in the modeling and parameterization of cloud properties and processes (e.g., Kessler 1969; Clark 1974; Lin et al. 1983; Rutledge and Hobbs 1983; Starr and Cox 1985; Cotton et al. 1986; Mitchell 1994; Pinto and Curry 1995; Fowler et al. 1996; Ryan 2000). A new impetus for bulk microphysical models was given recently by development of the double-moment bulk schemes that include prognostic equations for the number concentrations of hydrometeors in addition to the mixing ratio, which allows a higher accuracy in predicting the cloud microphysical properties (e.g., Ferrier 1994; Harrington et al. 1995; Meyers et al. 1997; Cohard and Pinty 2000; Girard and Curry 2001; Morrison et al. 2005a,b, Milbrandt and Yau 2005a, b).

A deficiency of empirically-derived parameterizations of particle size spectra is that the parameters are generally unknown and are fixed to some prescribed values. Experimental studies show wide variations of the relative dispersion (i.e., indices p) in clouds (e.g., Austin et al. 1985; Curry 1986; Mitchell 1994; Brenguier and Chaumat, 2001). Morrison et al. (2005a,b) and Morrison and Pinto (2005) calculated the values of p in a double-moment bulk microphysics scheme using analytical expressions from Khvorostyanov and Curry (1999b); these values showed substantial variations in time and space, resulting in variations in the onset of coalescence and in cloud optical properties.

Several attempts have been made to derive these spectra from kinetic equations or from equivalent approaches. Buikov (1961, 1963) formulated the first kinetic equations for the condensation growth and obtained their time-dependent analytical solutions in the diffusion and kinetic regimes. Srivastava (1969) derived the generalized gamma distribution (1.1) with $p = 2$ and $\lambda = 3$ for drops under the assumption that the cloud space is divided into a number of cells and the mass growth rate of each drop by diffusion is proportional to the volume of each cell.

Various versions of the stochastic kinetic equations of condensation have been derived (Levin and Sedunov 1966, Sedunov 1974, Voloshchuk and Sedunov 1977, Manton 1979, Jeffery et al. 2007; see reviews in Cotton and Anthes 1989; Khvorostyanov and Curry 1999a,b; Shaw 2003). Other approaches have also been developed, including Shannon's maximum entropy principle (Liu 1995; Liu et al. 1995; Liu and Hallett 1998), the Fokker-Plank equation in McGraw and Liu (2006), and averaging over the parcels with different ages in Considine and Curry (1996). Each of these approaches provides solutions for the small drop fraction in the form of gamma distribution (1.1), typically with values of $p = 1 - 2$ and $\lambda = p + 1$.

While these papers were able to derive gamma distributions similar to the observed droplet size spectra, they had the following deficiencies: the spectral parameter p was always fixed and the corresponding relative dispersions were constant and too high; the power of r in the exponential tail in (1.1) was always $\lambda = 2$ or 3, which is larger than the often observed value of $\lambda = 1$ (PK97). These solutions have only been rarely applied to crystalline clouds (e.g., Liu 1995).

Khvorostyanov and Curry (1999a,b, hereafter KC99a, KC99b) derived a version of the kinetic equation of stochastic condensation for the small-size droplet fraction in liquid clouds. This equation accounts for the nonconservativeness of supersaturation fluctuations and has a solution in the form of simple gamma distribution for particles with negligible fall velocities. In this paper, the kinetic equation from KC99a is extended to treat both small- and large-size fractions, and conditions relevant to ice clouds. The equation accounts for the coalescence/ aggregation process, allowing simultaneous consideration of condensation/deposition and aggregation. Analytical solutions are derived to the kinetic equation under various assumptions.

Part I addresses the small-size fraction and the companion paper by Khvorostyanov and Curry (2008, hereafter Part II) considers the large-size fraction. In particular, it is shown that all the aforementioned empirical distributions (generalized gamma, exponential and inverse power law) and their mixtures can be obtained as analytical solutions to the kinetic equation under various circumstances that include condensation and deposition, sedimentation, and aggregation. These results provide an internally consistent description of cloud particle spectra in both liquid and crystalline clouds over the extended size range of particles, providing a framework for relatively simple parameterization schemes that allows for variation in relative dispersion associated with the bulk environmental characteristics. Part I is organized as follows. Section 2 presents the basic equations and assumptions. In sections 3 and 4, the analytical solutions to the kinetic equations are obtained for various cases. Physical interpretation of the solutions is given in section 5, and an example of calculations for a crystalline cloud is presented in section 6. Section 7 is devoted to the summary and conclusions.

2. Basic equations, assumptions and simplifications

The basic equations developed here are applicable to pure liquid or pure crystalline clouds; mixed phase clouds are not explicitly addressed here. The kinetic equation of stochastic condensation derived in KC99a can be generalized by adding the collection (aggregation) and breakup terms $(\partial f/\partial t)_{col}$ and $(\partial f/\partial t)_{br}$ as

$$\frac{\partial f}{\partial t} + \frac{\partial}{\partial x_i}[(u_i - v(r)\delta_{i3})f] + \frac{\partial}{\partial r}(\dot{r}_{cond} f)$$

$$= \left(\frac{\partial}{\partial x_i} + \delta_{i3} G\vec{H}_L \frac{\partial}{\partial r}\right) k_{ij} \left(\frac{\partial}{\partial x_j} + \delta_{j3} G\vec{H}_R \frac{\partial}{\partial r}\right) f + \left(\frac{\partial f}{\partial t}\right)_{col} + \left(\frac{\partial f}{\partial t}\right)_{br}, \qquad (2.1)$$

where it is assumed that both liquid drops and ice crystals are represented by spheres of radius r. Here summation from 1 to 3 is assumed over doubled indices, t is time, x_i and u_i are the 3 coordinates and components of air velocity, $v(r)$ is the particle fall velocity, $\dot{r}_{cond}$ is the condensation (deposition) growth rate, δ_{i3} is the Kronecker symbol, and G is a parameter defined following KC99a. We introduce here the left operator $\vec{H}_L$, and the right operator $\overleftarrow{H}_R$, such that $\vec{H}_L k_{ij} = k_{ij}^n$, $k_{ij}^n = k_{ij}\overleftarrow{H}_R$, $\vec{H}_L k_{ij}\overleftarrow{H}_R = k_{ij}^{nn}$. These operators convert the conservative tensor, k_{ij}, into nonconservative tensors, k_{ij}^n, k_{ij}^{nn}, and commute with operators $\partial/\partial x_i$ and $\partial/\partial r$.

The conservative tensor k_{ij} is defined in KC99a and here as in the statistical theory of turbulence and is the integral over the Lagrangian correlation time T_L of the velocity correlation function $B_{ij}(t)$ that is expressed as the integral expansion of the spectral function $F_{ij}(\omega)$ over the turbulent frequencies ω (e.g., Monin and Yaglom 2007). The nonconservative tensors k_{ij}^n, k_{ij}^{nn} were derived in KC99a by generalizing the Prandtl's mixing length conception for the 4D space $(\vec{x}, r)$ and performing Reynolds averaging of the kinetic equation over the ensemble of turbulent fluctuations of the spectrum f', supersaturation S', and growth rate $\dot{r}'_{cond}$ and evaluating the correlations $< f'S' >$, $< \dot{r}'_{cond} f' >$, $< \dot{r}'_{cond} S' >$, $< S'S' >$ with account for nonconservativeness of supersaturation in fluctuations. Then k_{ij}^n arise as the time integral of the corresponding nonconservative correlation function B_{ij}^n that describes the correlation $\overline{u'_j S'}$, and the functions B_{ij}^{nn} and k_{ij}^{nn} arise from the autocorrelation $\overline{S'(t)S'(t_1)}$ of a nonconservative substance S'.

The turbulent coefficients k_{ij}^n and k_{ij}^{nn} involved in (2.1) and the correlation functions were derived in KC99a for pure liquid clouds; however, we have verified that the equations for pure crystalline clouds have the same form as the expressions derived previously for pure liquid clouds. The major difference between pure liquid and crystalline clouds is in the different values of supersaturation S (over water or ice in liquid or crystalline clouds), and in the supersaturation relaxation times τ_p

$$\tau_p = (4\pi D_v N\bar{r})^{-1} = \omega_p^{-1} , \tag{2.2}$$

where D_v is the vapor diffusion coefficient, N is the drop or crystal number concentration, $\bar{r}$ is their mean radius, and we introduced the inverse quantity $\omega_p = \tau_p^{-1} = 4\pi D_v N\bar{r}$ that can be called the "supersaturation relaxation frequency". The times τ_p determine the rate of supersaturation absorption and the "degree of nonconservativeness" of the substance (the drops or crystals) interacting with supersaturation.

For the turbulent frequencies ω that give the major contribution into the turbulent energy (e.g., Curry et al. 1988; Sassen et al. 1989; Quante and Starr 2002; Shaw 2003), the expressions derived in KC99a for the nonconservative turbulence coefficients show that $k_{ij}^{n}(\tau_p) \sim \omega_p^2 \sim \tau_p^{-2}$, and $k_{ij}^{nn}(\tau_p) \sim \omega_p^2 \sim \tau_p^{-2}$. That is, the nonconservative coefficients k_{ij}^{n}, k_{ij}^{nn} decrease with increasing τ_p and are generally smaller in crystalline clouds due to the greater τ_p than that in liquid clouds, which is caused by the different N, $\bar{r}$. The values of $\tau_p \sim 1$ - 10 s for liquid clouds with $N \sim 1\text{-}5\times10^2$ cm^{-3} and $\bar{r} \sim 5$ - 10 μm. Calculations of τ_p in cirrus and mid-level ice clouds using spectral bin models show that it varies in the range 10^2 - 10^4 s for typical N and $\bar{r}$ (e.g., Khvorostyanov and Sassen (1998, 2002); Khvorostyanov, Curry et al. (2001); Sassen and Khvorostyanov (2007)). Thus, the values of $k_{ij}^{n}(\tau_p)$, $k_{ij}^{nn}(\tau_p)$ are smaller for crystalline clouds than for liquid clouds but estimation from the equations in KC99a shows that values of $k_{ij}^{n}(\tau_p)$, $k_{ij}^{nn}(\tau_p)$ are comparable for both liquid and crystalline clouds.

Analytical solutions to the kinetic equation (2.1) can be obtained with the following additional assumptions and simplifications:

1) The cloud is quasi-steady state, $\partial f/\partial t = 0$. This does not imply complete steady state, and the time dependence can be accounted for via the integral parameters in the solution.

2) The cloud is horizontally homogeneous, $\partial f/\partial x = \partial f/\partial y = 0$.

3) The size spectrum is divided into 2 size regions,

$$f(r) = \begin{cases} f_s(r), & r < r_0, \\ f_l(r), & r > r_0, \end{cases} \tag{2.3}$$

where $f_s(r)$ and $f_l(r)$ are the small-size and large-size fractions, and r_0 is the boundary radius between the two size fractions. The value of r_0 ~ 30 - 50 μm for the drops and ~30-80 μm (or maximum dimension D_0 ~ 60-160 μm) for the crystals; r_0 separates the domain $r < r_0$ where accretion rates are small and particles growth is governed mostly by the condensation/deposition from the domain $r > r_0$ where collection rates become important and prevail (see e.g., Cotton and Anthes 1989, pp. 90-94). The functions $f_s(r)$ and $f_l(r)$ corresponds to the bulk categorization of the condensed phase into cloud water and rain for the liquid phase and cloud ice and snow for the crystalline phase.

4) The nonconservative turbulence coefficients are parameterized following KC99a to be proportional to the conservative coefficient k as $k_{ij}^{n} = c_n k$, and $k_{ij}^{nn} = c_{nn} k$. In general, c_n, c_{nn} have values that are smaller than but close to unity; they are smaller in crystalline than in liquid clouds.

5) The coagulation term $(\partial f/\partial t)_{col}$ is described in detail in Part II and we assume that drop breakup does not influence the small fraction. The coagulation-accretion growth rate (both for the drop collision-coalescence and for the crystal aggregation with crystals) is considered in the continuous growth approximation (Cotton and Anthes 1989; PK97, Seinfeld and Pandis 1998), with account for only the collision-coalescence between the particles of the different fractions of the spectrum, $f_s(r)$ and $f_l(r)$. The decrease in small fraction f_s is described in this approximation as collection of the small-size fraction by the large-size fraction.

$$\left(\frac{\partial f_s}{\partial t}\right)_{col} = -I_{loss} = -\sigma_{col} f_s, \qquad r < r_0 \quad , \tag{2.4}$$

$$\sigma_{col} = \pi E_c \int_{r_0}^{\infty} r^2 v(r) f_l(r) dr \tag{2.5}$$

These equations are derived in Part 2 from the Smoluchowski stochastic coagulation equation along with the mass conservation at the transition between the small- and large-size fractions.

With these assumptions, the kinetic equation (2.1) can be written for f_s:

$$\frac{\partial}{\partial z}[(w - v(r))f_s] + \frac{\partial}{\partial r}(\dot{r}_{cond} f_s) = k\frac{\partial^2 f_s}{\partial z^2}$$

$$+ c_n kG\left(\frac{\partial^2 f_s}{\partial r \partial z} + \frac{\partial^2 f_s}{\partial z \partial r}\right) + c_{nn} kG^2 \frac{\partial^2 f_s}{\partial r^2} - \sigma_{col} f_s, \qquad (2.6)$$

All of the quantities on the left-hand side (f, w, S) indicate averaged values in the sense discussed in KC99a,b, and all fluctuations are included on the right-hand side of the equation. The terms on the left-hand side describe convective and sedimentation fluxes and drop (crystal) condensation (depositional) growth/evaporation, and the terms on the right-hand side describe turbulent transport, stochastic effects of condensation/deposition growth and absorption by the large-size fraction.

To enable analytic solutions to (2.6), we make the following additional assumptions:

6) The vertical gradient of f_s can be parameterized as a separable function:

$$\frac{\partial f_s(r,z)}{\partial z} = \alpha_s(z)\varsigma(r) f_s(r,z). \qquad (2.7a)$$

The functions $\alpha_s(z)$ and the $\zeta_s(r)$ can be different for each fraction, determining the magnitude of the gradient and its possible radius dependence. If $\zeta_s(r) = 1$, and

$$df / dz = \alpha_s f \,, \qquad (2.7b)$$

it is easily shown from the definition of liquid (ice) water content that

$$\alpha_s(z) = (1/q_{ls})(dq_{ls}/dz). \qquad (2.8)$$

7) We assume that terminal velocity $v(r)$ can be parameterized following Khvorostyanov and Curry (2002, 2005) in the form

$$v(r) = A_v(r) r^{B_v(r)}, \qquad (2.9)$$

where $A_v(r)$ and $B_v(r)$ are continuous functions of particle size, that include consideration of various crystal habits and non-spherical drops and turbulent corrections to the flow around the particles.

8) The condensation or deposition growth/evaporation rate $\dot{r}_{cond}$ is described by the simplified Maxwell equation

$$\dot{r}_{cond} = \frac{bS}{r}, \qquad b = \frac{D_v \rho_{vs}}{\Gamma_p \rho_w}, \tag{2.10}$$

where $S = (\rho_v - \rho_{vs})/\rho_{vs}$ is supersaturation over water (ice), ρ_v and ρ_{vs} are the environmental and saturated over water (ice) vapor densities, ρ_w is the water (ice) density, and Γ_p is the psychrometric correction associated with the latent heat of condensation.

Assuming $\zeta(r) = 1$, and substituting (2.7b) - (2.10) into (2.6) allows elimination of z-derivatives and we obtain a differential equation that is only a function of r:

$$c_{nn} k G^2 \frac{d^2 f_s}{dr^2} + \left[2c_n k G \alpha_s - \frac{bS}{r} \right] \frac{df_s}{dr}$$

$$+ \left[2c_n k G \alpha_s + \alpha_s^2 k + \frac{d(\alpha_s k)}{dz} - \alpha_s (w - v) - \frac{dw}{dz} - \sigma_{col} + \frac{bS}{r^2} \right] f_s = 0. \tag{2.11}$$

The dimensionless parameter G was derived in KC99a,b in the process of averaging over the turbulence spectrum, and can be written in various forms:

$$G = \frac{\rho_a}{\rho_w} \frac{c_p}{L} \frac{\gamma_d - \gamma_w}{4\pi N \bar{r}^2} \approx \frac{c_f}{3} \frac{\rho_a c_p (\gamma_d - \gamma_w)}{L} \frac{\bar{r}}{q_{ls}} \tag{2.12}$$

where c_p is the specific heat capacity, L is the latent heat of condensation or deposition, γ_d and γ_w are the dry and wet (water or ice) adiabatic lapse rates, ρ_a is the air density, N and $\bar{r}$ are number concentration and mean radius of the particles, q_{ls} is the liquid (ice) water content of the small fraction. The coefficient c_f occurs as we use a relation $q_{ls} = (4/3)\pi c_f \rho_w N \bar{r}^3$, or $(4\pi N \bar{r}^2)^{-1} = (c_f/3)\rho_w \bar{r}/q_{ls}$; c_f depends on the shape of the spectra and is close to 1. E.g., for gamma distributions with the index p considered below, $c_f = (p+2)(p+3)/(p+1)^2$, i.e., $c_f/3$ varies from 1 for $p = 1$ to 0.5 for $p = 6$. In the future, we assume in (2.12a) $c_f/3 \approx 1$, since its variations are several orders of magnitude smaller than variations of q_{ls}, N, and $\bar{r}$. Introducing the adiabatic liquid (ice) water content $q_{ls,ad}(z) = (dq_{ls}/dz)_{ad}(z - z_{bot})$, where $(dq_{ls}/dz)_{ad}$ is its vertical gradient (Curry and Webster 1999)

$$\left(\frac{dq_{ls}}{dz}\right)_{ad} = \frac{c_p}{L}(\gamma_d - \gamma_w)\rho_a, \tag{2.13}$$

z_{bot} is the height of cloud bottom and $(z - z_{bot})$ is altitude above z_{bot}, (2.12) can be also rewritten as

$$G = \frac{\bar{r}}{q_{ls}/(dq_{ls}/dz)_{ad}} = \frac{\bar{r}}{(z - z_{bot})} \cdot \left(\frac{q_{ls}}{q_{ls,ad}}\right)^{-1}. \tag{2.14}$$

The quasi-steady supersaturation S_q can be written following KC99a,b:

$$S_q = A\tau_p w_{ef}, \qquad A = \frac{c_p}{L}\Gamma_p \frac{\rho_a}{\rho_{vs}}(\gamma_d - \gamma_w), \tag{2.15}$$

where τ_p is the supersaturation relaxation time (2.2) and the w_{ef} is the effective vertical velocity described by KC99a,b. Then the condensation term (2.10) can be rewritten as

$$\dot{r}_{cond} = \frac{bS_q}{r} = \frac{c_{con} w_{ef}}{r}, \tag{2.16}$$

$$c_{con} = G\bar{r} = bA\tau_p = D_v \frac{\rho_a}{\rho_w} \frac{c_p}{L} \frac{(\gamma_d - \gamma_w)}{4\pi D_v N\bar{r}}. \tag{2.17}$$

3. Solution neglecting the diffusional growth of larger particles

In some situations, it can be assumed that the terms in (2.11) with diffusional growth can be neglected for the larger particles in the small-size fraction. These terms can be much smaller in the tails of the spectra than the other terms in (2.11) for small values of super- or subsaturation, or for sufficiently large gradients α_s in relatively thin clouds, or for sufficiently large values of G. This allows for neglect in (2.11) of the diffusional growth terms in the tails of the spectra since they decrease with radius faster than the other terms. We obtain asymptotic solutions in the small and large particle limits, and then merge these two solutions, to obtain the solution neglecting the diffusional growth of larger particles.

3.1 Solution at small *r*

The solution of (2.11) at small r is obtained in Appendix A in the form of a power law

$$f_s(r) \sim r^p \,, \tag{3.1}$$

where the index p is

$$p = \frac{bS}{c_{nn} k G^2} \,. \tag{3.2}$$

Eq. (3.2) is a generalization of the corresponding solution from KC99b where the index p was expressed via the mean effective vertical velocity under assumption of quasi-state state supersaturation (2.15). Now, (3.2) accounts for various possible sources of supersaturation (advective, convective, radiative, mixing among the parcels and with environment). In cloud layers with positive supersaturation, $S > 0$, then $p > 0$, and (3.1) has the form of the left branch of the gamma distribution (for r smaller than the modal radius). In evaporating cloud layers with negative supersaturation, $S < 0$, then $p < 0$ and the solutions have the form of the inverse power laws.

3.2 Solution at large *r*

The solution for the larger particles in the small-size fraction (but $r < r_0$) is found in Appendix A similar to KC99b as the exponential function:

$$f_s(r) \propto \exp(-\beta_s r) \,, \tag{3.3}$$

where β_s is a solution of the quadratic equation with the 2 roots

$$\beta_{s,1,2} = \frac{c_n k \alpha_s \mp \left(c_n^2 k^2 \alpha_s^2 - c_{nn} k^2 \alpha_s^2 (1-\mu_s^2)\right)^{1/2}}{c_{nn} k G} \,, \tag{3.4}$$

and

$$\mu_s = \left[\frac{1}{\alpha_s^2 k} \left(\alpha_s (w - v) + \frac{dw}{dz} + \sigma_{col} - \frac{d\alpha_s k}{dz} \right) \right]^{1/2} . \tag{3.5}$$

The solutions are simplified if the nonconservativeness of *k*-components is neglected, $c_{nn} = c_n = 1$:

$$\beta_{s,1,2} = \frac{\alpha_s}{G} (1 \mp \mu_s) . \tag{3.6}$$

Hereafter in this section, the negative and positive signs relate to the 1st and 2nd solutions respectively. Eq. (3.3) represents the exponential tail of the spectrum and the slopes (3.4), (3.6) are generalizations of the corresponding expression from KC99b with account for coagulation/accretion and vertical gradients of k, w, α_s. Physical conditions require that $\beta_{s,1,2} > 0$.

3.3 Merged solution

From the two asymptotic solutions, the general solution to (2.11) neglecting the diffusional growth of large particles can be found following KC99b to be of the form

$$f_s(r) = c_{1,2} r^p \exp(-\beta_{s,1,2} r) \Phi(r) . \tag{3.7}$$

Substituting (3.7) into (2.11) yields the confluent hypergeometric equation for Φ with two solutions that are Kummer functions (described in detail in Appendix A). Then the complete solutions for these cases with correct asymptotics at small and large r are

$$f_{s,1,2}(r) = c_{1,2} r^p \exp\left(-\frac{\alpha_s}{G} (1 \mp \mu_s) \right)$$

$$\times F\left(\frac{p}{2\mu_s} (\mu_s \pm 1), p; \mp \frac{2\alpha_s \mu_s}{G} r \right), \tag{3.8}$$

where $F(a,b;x)$ is the Kummer (confluent hypergeometric) function. These solutions are derived in Appendix A assuming v = const, μ_s = const. Now, the correction for $v(r)$ can be introduced into (3.8) using the real fallspeed $v(r)$, and the solution is valid at such r that $\mu_s^2 > 0$. Evaluation of the normalizing constants $c_{1,2}$, moments, and asymptotics of these solutions are described in KC99b.

Equation (3.8) is similar to a gamma distribution with some modifications that generalize the solutions from KC99b. The left branch of these gamma distribution type spectra is described by the index p, which is now sign-variable, depending on supersaturation and allows for various sources of cooling. It was found in KC99b that there are 2 asymptotics of solutions of the type (3.8) for sufficiently small or large q_{ls} (e.g., near the boundaries or the center of the cloud), where the Kummer functions are reduced to the product of the power law and exponent and (3.8) is reduced to the gamma distribution (3.7) with $\Phi = 1$ but with modified p, β_s. These asymptotics can be generalized using the new formulation to account for sedimentation, accretion and gradients of w and k.

4. Solution including the diffusional growth of large particles

The solution obtained in section 3 assumed that the diffusion growth terms are small at sufficiently large r. However, if these terms are still significant in the tail of the small-size fraction, as it can be at large sub- and supersaturations, we must seek another solution that accounts for these terms. We again consider the two asymptotic cases at small and large r (again, within the small-size fraction).

At small r, the same most singular terms in (2.11) give the main contribution, and the solution is the same power law (3.1), $f_s \sim r^p$, with the index p defined in (3.2). At large r, if the diffusional growth terms are retained, then (2.11) is a 2nd order differential equation with rather complicated variable coefficients, and an analytical solution is not easily obtained. Hence, we seek a simplification that will enable an analytical solution. At large r, it is reasonable to assume that the tail of the spectrum is smooth and the r-gradients of the spectrum are smaller than near the mode. Then we can neglect in (2.11) the stochastic diffusion terms in radii-space (the terms with G), and arrive at the following equation

$$[w - v(r)]\alpha_s f_s + \frac{dw}{dz} f_s + bS \frac{d}{dr}\left(\frac{f_s}{r}\right)$$

$$=\left[\alpha_s^2 k+\alpha_s \frac{dk}{dz}+k\frac{d\alpha_s}{dz}-\sigma_{col}\right]f_s \tag{4.1}$$

A solution to this equation is found in Appendix B

$$f_s(r)=\frac{r}{r_1}f_s(r_1)\exp\{-[\beta_{s2}(r)r^2-\beta_{s2}(r_1)r_1^2\}, \tag{4.2}$$

where the slope β_{s2} is

$$\beta_{s2}(r)=\frac{1}{bS}\left(\frac{\alpha_s w+dw/dz+\sigma_{col}-\alpha_s^2 k-\alpha_s k'-k\alpha_s'}{2}-\frac{\alpha_s v(r)}{B_v+2}\right), \tag{4.3}$$

and the primes denote here derivatives by z. This is the solution for the tail of the small fraction. Eq. (4.2) can be written in a slightly different form that includes the terms with r_1 in the normalizing constant c_N

$$f_s(r)=c_N r\exp[-\beta_{s2}(r)r^2]. \tag{4.4}$$

The merged solution can be constructed again as in section 3 as an interpolation between the two asymptotic regimes at small and large r:

$$f_s(r)=c_N r^p\exp[-\beta_{s2}(r)r^2]\Phi(r). \tag{4.5}$$

Unfortunately, the resulting equation for Φ in this case is much more complicated than the confluent hypergeometric equation in section 3 and its solutions cannot be reduced to Kummer functions. Thus, (4.5) can be used with some interpolation formulae for Φ, e.g.,

$$\Phi(r)=\exp(-r/r_{sc})+(r/r_{sc})^{1-p}\tanh(r/r_{sc}), \tag{4.6}$$

where r_{sc} is a scaling radius comparable with $\bar{r}$. At $r << r_{sc}$, the first term tends to 1, the 2nd term tends to 0, and we obtain from (4.5) $f_s \sim r^p$ at small r since $\beta_{s2}(r)r^2 << 1$ in (4.5) and exp $\to$ 1. At $r >> r_{sc}$, the solution (4.5) tends to (4.4). Thus, (4.5) ensures correct limits at both small and large r.

An advantage of (4.5) is that the tail of the spectrum explicitly accounts for the diffusional growth process. This results in the inverse dependence of the slope β_{s2} (4.3) on supersaturation; that is, the slope becomes steeper as $|S|$ increases. This is physically justified since more vigorous condensation/evaporation should produce narrower spectra. At sufficiently large r, the 2nd term with $v(r)$ in (4.3) dominates, and the slope is

$$\beta_{s2} = -\frac{\alpha_s v(r)}{bS(B_v + 2)} . \tag{4.7}$$

Since f_s should decrease at large r, the slope β_{s2} should be positive. Therefore, the terms α_s and S should have opposite signs, i.e., $\alpha_s < 0$ and LWC (IWC) increases downward in the growth layer ($S > 0$, $\alpha_s < 0$), and decreases downward in the evaporation layer ($S < 0$, $\alpha_s > 0$), which is physically justified for this limit $v(r) >> w$. The argument in the exponent is $\beta_{s2} r^2 \sim r^2 v(r) \sim r^{B_v+2}$, i.e., the tails of the spectra with $v(r) \sim r^2$, $\sim r$ and $\sim r^{1/2}$ (e.g., Rogers 1979; KC05), decrease as $\exp(-r^4)$, $\exp(-r^3)$, and $\exp(-r^{2.5})$, respectively. That is, a larger value of the fall velocity $v(r)$ is associated with a greater slope and shorter tail, which is consistent with increased precipitation from the tail.

When $v(r)$ is small relative to the other terms (e.g., $v(r) << |w|$), the exponent β_{s2} is determined by the 1st term in parentheses (4.3); neglecting for simplicity w', k', α_s', we obtain

$$\beta_{s2} = \frac{1}{2bS}(\alpha_s w + \sigma_{col} - \alpha_s^2 k) . \tag{4.8}$$

Again, the signs of S and of expression in parentheses should coincide to obtain $\beta_{s2} > 0$. In particular, if $S > 0$, $w > 0$, and the term $\alpha_s w$ is greater than σ_{col} and $\alpha_s^2 k$ in (4.8), then $\alpha_s > 0$, i.e., q_{ls} increases with height, which is justified for this limit $w >> v(r)$. In this case, the slope becomes steeper (spectrum narrows) when w increases (as in regular condensation), and when σ_{col} increases (faster absorption by the large fraction), and β_{s2} decreases when k increases (turbulence causes broadening of the spectra). Since β_{s2} does not depend on r for this case, the tail of the spectrum decreases as $\exp(-r^2)$.

The merged solution (4.5) differs from those found previously in the following ways. At small r, the solution is a power law with variable rather than fixed index p, allowing variable relative dispersions. Also, the slope of the tail is not constant but varies (generally increases) with r; accounting for the greater depletion of large particles with greater sedimentation rate and includes depletion of the small fraction due to accumulation by the large fraction. The tail (4.4) at large r behaves as exp($-r^{\lambda}$) with λ varying from 2 to 4 for various situations, in broad agreement with the range of values determined by previous analytical solutions.

5. Physical interpretation of the parameters

The general equation (3.2) shows that the index $p \sim S$, and hence p can be positive or negative. These two cases are considered below.

a) $p > 0$, gamma distributions

If the major source of supersaturation is uplift and/or radiative cooling, then p can be expressed similar to KC99a,b via the "effective" vertical velocity w_{ef}, using (2.15) - (2.17),

$$p = \frac{c_{con} w_{ef}}{c_{nn} k G^2} = \frac{\bar{r} w_{ef}}{c_{nn} k G} . \quad (5.1)$$

The term "effective" here means subgrid velocities with addition of the "radiative-effective" velocities w_{rad} introduced in KC99a,b that allow direct comparison of the dynamical and radiative cooling rates

$$w_{ef} \approx w' + w_{rad} , \qquad w_{rad} = -(1/\gamma_a)(\partial T/\partial t)_{rad} , \quad (5.2)$$

where $(\partial T/\partial t)_{rad}$ is the radiative cooling rate caused by the total radiative flux divergence. Morrison et al. (2005a, b), and Morrison and Pinto (2005) used (5.1), (5.2) to evaluate p-indices of the gamma distributions in a bulk double-moment cloud model. They specified the subgrid velocities w' similar to Ghan et al. (1997) via the turbulent coefficient k and mixing length l_{mix}:

$$w' \approx k / l_{mix} . \quad (5.3)$$

Using (2.12) - (2.14) for G, the index p from (5.1) can be written also in the following forms

$$p = \frac{w_{ef}}{c_{nn}k} \frac{L}{c_p(\gamma_d - \gamma_w)} \frac{4\pi\rho_w N\bar{r}^3}{\rho_a} \approx \frac{w_{ef}}{c_{nn}k} \frac{q_{ls}}{(dq_{ls,ad}/dz)} \approx \frac{w_{ef}}{c_{nn}k} \chi_{ad}\, \Delta z \,, \qquad (5.4)$$

where $\chi_{ad} = q_{ls}/q_{ls,,ad}$ is the adiabatic liquid (ice) ratio, and $\Delta z = z - z_{bot}$ is the height above cloud base. All of the parameters in (5.4) are available in the bulk models, and the index p can be easily calculated. The first expression in (5.4) can be used in the double-moment models, when both q_{ls} and N are known, then $\bar{r}$ and p can be calculated (e.g., Morrison et al. 2005a, b). The 2nd and 3rd expressions in (5.4) can be used in single moment models, when only q_{ls} is available.

If $w_{ef} > 0$, then p is positive. Equations from sections 3and 4 show that the size spectrum of the small fraction is then the power law multiplied by the exponent, i.e., a gamma distribution. The expressions (5.4) for this case show that p depends on 5 factors: w, k, adiabatic ratio χ_{ad}, height Δz, and c_{nn}.

These equations indicate several features that are similar for both cloud drop and crystal size spectra. Eqs. (5.1), (5.4) show that p increases (spectra become narrower) when positive w_{ef} increases, which is similar to the effect of regular condensation, and p decreases (spectra broaden) when k increases, which describes the effect of turbulence in stochastic condensation. The additional factor in (5.4) is the adiabatic ratio χ_{ad}. In convective clouds, χ_{ad} usually decreases with height above cloud base due to entrainment. This may cause a decrease of p and broadening of the spectra with height in the lower cloud layers. In the upper cloud half, χ_{ad} may tend to nearly constant values (e.g., PK97), while the height-factor Δz causes a counter-effect in (5.4), causing increase of p and spectral narrowing. Which effect will dominate, depends on the product $\chi_{ad}\cdot\Delta z$. If χ_{ad} decreases with height faster than $1/\Delta z$, then $\chi_{ad}\cdot\Delta z$ decreases and the spectra broaden with height as was observed in a convective cloud by Warner (1969). It is this effect that is in contradiction with the theory of regular condensation that predicts narrowing of the spectra with height, and stimulated numerous attempts to explain the broad spectra including the stochastic condensation theory as reviewed in Introduction.

However, later experimental studies showed that broadening with height is not a common feature of the droplet spectra. If χ_{ad} in (5.4) decreases with height slower than $1/\Delta z$, then $\chi_{ad}\cdot\Delta z$ increases and the spectra narrow with height, resembling the effect of regular condensation, as observed in a shallow convective cloud by Austin et al. (1985). The values of relative dispersion σ_r for a convective cloud described in Austin et al. (1985) varied from σ_r = 0.2 - 0.3 in the middle of the cloud (corresponding p calculated from (1.3) are 13-25) to σ_r = 0.17 - 0.21 (p = 22 -35) near cloud top. Thus, the spectra narrow with height in this case, in contrast to the convective cloud observed by Warner (1969). If the product $\chi\cdot\Delta z$ is close to but slightly lower than the adiabatic value, such as in convective adiabatic cores due to lateral mixing (i. e., $\chi_{ad}\cdot\Delta z \approx$ const), then the spectra can be narrow, but still wider than would be in adiabatic ascent, similar to the situation observed by Brenguier and Chaumat (2001) in cumulus clouds.

It was shown in KC99b that if the profiles of LWC (or IWC) are close to adiabatic, $\chi_{ad} \approx 1$, this situation is equivalent to the absence of turbulence, $k = 0$, and the spectra should be narrow. A good illustration can be found in Liu and Hallett (1998), who showed the very narrow size spectra in a lenticular cloud over the Sierra Nevada formed adiabatically in a laminar flow.

In low-level St-Sc clouds, radiative cooling plays substantial role in formation of particles spectra. Eq. (5.2) shows that the w_{rad} reach maxima in the layers of maximum radiative cooling. The longwave cooling rates of 80 - 120 K day^{-1} are often measured and calculated in the upper layers of St-Sc, about 50-70 m below cloud top (e.g., Curry 1986; Cotton and Anthes 1989; KC99b). The w_{rad} calculated with (5.2) reach 9-12 cm s^{-1} and can exceed the dynamical vertical velocities in these layers. The values of w_{eff} and the indices p are maximum, and σ_r are minimum just below cloud top. The values of p calculated in KC99b and in Morrison et al. (2005a) with (5.4) for liquid arctic stratus cloud described in Curry (1986) were in the range 5-10 with corresponding relative dispersions σ_r = 0.3 - 0.5, with minimum values in the layers of maximum radiative cooling, close to the values and profiles observed in Curry (1986).

Note that the version of the stochastic condensation theory developed in KC99a,b and here allows p and σ_r to vary with height and such low values of $\sigma_r \sim 0.15$ -0.3 observed by Austin et al. (1985), Curry (1986) and others, as well as substantially higher σ_r = const = 0.71 with $p = 1$ and $\sigma_r = 0.58$ with $p = 2$ predicted by some cited theories of stochastic condensation.

Relative to the spectra of water drops, different features of the crystal size spectra arise in this parameterization by the different values of N, $\bar{r}$, and lapse rates γ_w. In liquid clouds, $N \sim$ 1-5 $\times 10^2$ cm^{-3}, $\bar{r} \sim$ 5-10 μm, and according to (2.12), $G \sim (0.3 - 5)\times 10^{-8}$. In crystalline cirrus clouds with $N \sim (1\text{-}5)\times 10^2$ L^{-1} (~ 3 orders of magnitude smaller than droplet concentrations), $q_{ls} \sim$ 10-20 mg m^{-3}, $\bar{r} \sim$ 50-100 μm, and (2.12) yields $G \sim 10^{-7}$- 10^{-5}. Thus, both G and $\bar{r}$ are 1-2 orders greater in cirrus than in liquid clouds. According to (5.1), $p \sim \bar{r}/G$, so that the increase in G is compensated by a similar growth in $\bar{r}$, and the indices p appear to be comparable in liquid and crystalline clouds, as illustrated in more detail in section 6.

According to (5.4), $p \sim (\gamma_d - \gamma_w)^{-1}$. Since $\sigma_r = (p + 1)^{-1/2}$, then for the typical condition $p >> 1$, $\sigma_r \approx p^{-1/2} \sim (\gamma_d - \gamma_w)^{1/2}$. The wet adiabatic lapse rate γ_w tends to the dry adiabat γ_d with decreasing temperature; thus, p increases and σ_r decreases at low T. This explains observed (e.g., Herman and Curry 1984) narrower spectra in cold liquid As-Ac clouds at $T \sim$ -20 ºC, P = 800 hPa ($\gamma_d - \gamma_w$ = 1.7 ºC km^{-1}) than in warmer Sc at $T \sim$ 0ºC ($\gamma_a - \gamma_w$ = 4 ºC km^{-1}). This dependence is also strong in cirrus clouds at low temperatures for the wet adiabat γ_w over ice, e.g., at a pressure P = 200 hPa, the value $\gamma_d - \gamma_w$ = 4.14 ºC km^{-1} at -20 ºC, 1.22 ºC km^{-1} at -40 ºC, and 0.62 ºC km^{-1} at -50 ºC. Thus, (5.4) predicts that the index p would increase by a factor of ~7 from -20 ºC to -50 ºC if N, $\bar{r}$, and pressure were the same, and the crystal size spectra in cirrus should become narrower with decreasing T. This feature is seen in the experimental data where the spectra are sorted by temperature or height (e.g., Heymsfield and Platt 1984; Sassen et al. 1989; Platt 1997; Poellot et al. 1999, Lawson et al. 2006), but, to our knowledge, has not been previously explained. This theory provides a basis for the quantitative description of the temperature dependence of the drop and crystal size spectra. Note that this narrowing of the spectra with decreasing T causes slower droplet freezing, droplet and crystal precipitation, and coagulation-accretion, that is, greater colloidal stability of the colder clouds.

b) p < 0, inverse power law distributions

Eq. (3.2) predicts that the index p is negative in cloud layers with subsaturation, $S < 0$. Subsaturation may occur in a cloud due to downdrafts, advection of drier or warmer air, entrainment of dry ambient air, and radiative heating. Under these conditions, the smallest particles should have been evaporated to some boundary values r_* and the left branch at $r > r_*$ is described by the inverse power law

$$f_s(r) \sim (r/r_*)^p \sim (r_*/r)^{-|p|}, \tag{5.5}$$

which coincides with (1.4). Such inverse power laws have been found by fitting experimental data from crystalline (cirrus and frontal) clouds in HP84, Platt (1997), Poellot et al. (1999), Ryan (2000), and in the data from liquid clouds in the works cited in Introduction. Here, this inverse power law is obtained as a solution to the kinetic equation and its index p is expressed in (3.2) via physical cloud parameters.

An estimation of p from (3.2) for cirrus clouds shows that at $T \sim$ -40ºC with k = 5 - 10 m^2 s^{-1} and $G \sim 1\text{-}\ 2\times10^{-7}$, the parameters are $kG^2 \sim 0.5\text{-}1\times10^{-9}$ cm^2 s^{-1}, $b \sim 4\times10^{-8}$ cm^2 s^{-1}. Then at subsaturation S = - 0.1 (- 10 %), assuming $c_{nn} = 1$, we obtain $p = bS/kG^2 \sim$ -2 - 4. The indices estimated here are quite comparable to those in HP84, Platt (1997), Poellot et al. (1999), and Ryan (2000) that give $p \sim$ -1 to -8. In all the works where the size spectra are sorted by temperature, there is distinct increase of the measured and fitted slopes $|p|$ with decreasing temperature. This also can be described using (5.4) with $w_{ef} < 0$. Then again, as in the case $p > 0$, the slopes $|p| \sim (\gamma_d - \gamma_w)^{-1}$. Comparing the spectra at two temperatures, -20 ºC (P = 600 hPa, $-\gamma_d - \gamma_w$ = 2.14 ºC km^{-1}) and -50 ºC (P = 200 hPa, , $\gamma_d - \gamma_w$ = 0.62 ºC km^{-1}), we obtain that the slopes $|p|$

should be about 2.14/0.62 = 3.5 times larger at colder temperature if the other parameters are the same. A more precise evaluation for various P, T, N, $\bar{r}$ can be performed using (5.4) instead of fitting to the measured spectra as it is usually done.

Note that the subsaturated layers with negative p may constitute significant portions of crystalline clouds, particularly as falling particles enter the subsaturated regions below the cloud. Hall and Pruppacher (1976) showed that falling crystals can survive at subsaturation over 2-6 km, which was confirmed by later modeling studies of evolving cirrus (e.g., Jensen et al. 1994; Khvorostyanov and Sassen 1998, 2002, hereafter KS98, KS02; Khvorostyanov, Curry et al. 2001). The life cycle of cirrus clouds usually begins with ice nucleation on haze particles that requires some threshold supersaturation. After this threshold has been reached, the rate of vapor absorption by the crystals may exceed the rate of supersaturation generation, so that the mean supersaturation decreases, the thickness of cloud evaporation layer increases and can exceed the thickness of the growth layer. This process, governed by the crystal supersaturation relaxation time, is slow and may last up to several hours. This may cause significant frequency of ice subsaturated (evaporation) layers in crystalline clouds and explain observations of the inverse power law spectra of HP84 type, based on the results of this section.

All these features of the spectra discussed in this section and related to variations of the indices p are ignored and missed in models with parameterizations that use constant values of p = 0 - 3 for all spectra. This may substantially reduce the accuracy of such models.

The measured and calculated values of p, σ_r have strong dependence on the scales of averaging L_x: σ_r increases and p decreases with increasing L_x (see, e.g., discussions in Cotton and Anthes 1989; Liu and Hallett 1998). This effect is well described by our model and (5.1)-(5.4), since averaging over large horizontal scales or grid boxes may lead to a substantial decrease in w_{ef}, up to an order of magnitude (Cotton and Anthes 1989). This causes corresponding decrease in S, and, according to (5.1), in p. The estimates in KC99b showed that p calculated with w_{ef} typical of “local” scales were p ~ 5-20 with corresponding σ_r ~ 0.2-0.3, but p calculated with w_{ef} typical of meso- or synoptic scales were p ~ 1-2, with corresponding σ_r ~ 0.6-0.7. This dependence on the scale L_x was convincingly illustrated, e.g., in Noonkester (1984) who showed that the droplet spectra sampled in the middle layer of the California stratus on the scales ~ 0.5 km have the relative dispersions σ_r ~ 0.21 - 0.37 (i.e., p ~ 21 to 6), and sampling at the same levels but on the scales ~ 6.4 km yields a significant increase in σ_r ~ 0.66 - 0.78 (decrease in p ~ 1.3 to 0.6).

It should be emphasized that the local narrow spectra with p ~ 6 - 20, as all the cited experimental data indicate, are representative of the cloud processes and should be used in parameterizations, since these local spectra govern radiative transfer, coagulation-accretion, and precipitation. Averaging over large scales leads to an artificial broadening of the spectra, and unphysical lowering of the indices p to the values of 1-2; use of such broad spectra may cause artificial acceleration of the coagulation processes, faster precipitation formation and cloud dissipation, and the errors in evaluation of the radiative scattering and absorption coefficients.

6. Calculation of size spectra for a crystalline cloud

Examples of calculations of the size spectra for liquid clouds based on stochastic condensation theory were given in KC99b, and here we present calculations of the spectra and their parameters for a crystalline cloud. Calculations are performed using 4 different input profiles. The baseline profiles approximate a 2 -layer cloud of cirrus and nimbostratus observed on July 8 1998 in SHEBA-FIRE field campaign in the Arctic and simulated with bin microphysics model in Khvorostyanov, Curry et al. (2001, hereafter KCetal01). The cloud shown in Fig. 1 is pure crystalline, the small fraction exists in the region between 4 and 10 km with maximum IWC q_{ls} = 20 mg m^{-3} at 7 km and maximum crystal concentration N_i ~ 90 L^{-1} at 9 km; and the mean crystal radius $\bar{r}$ increases from 30 μm near cloud top to about 90 μm at the bottom. The ice supersaturation is assumed constant at S = -15 % below 7.2 km, increasing from 0 at 7.2

km to maximum of 12 % at 9 km and then decreasing to - 80 % (Fig. 1c). This design of S is consistent with observations (e.g. Jensen et al. 2001) and detailed simulations using a model with spectral bin microphysics and supersaturation equation in KCetal01, KS98 and KS02, which showed that the maximum IWC in cirrus can be located near $S = 0$, since IWC increases downward in all the layer with $S > 0$. Maxima in S and N_i may coincide, reflecting the mechanism of ice nucleation governed by supersaturation. The values of α_s calculated from (2.8) are positive below the level of maximum IWC and are negative above, with extremes of about $\pm$ 2 km^{-1} (Fig. 1d). We used the constant values of w = 3 cm s^{-1} and k = 5 m^2 s^{-1}. These profiles are referred hereafter as the baseline (case 1) and denoted in the legends as "Base". To test the sensitivity of the results to the input profiles, the same calculations were performed with the following changes: doubled IWC and $\bar{r}$ (case 2); same IWC as in the baseline case but doubled $\bar{r}$ (case 3); and same conditions as the baseline case but with doubled k (case 4).

Profiles of the parameter G calculated with (2.12) and these input data are shown in Fig. 2a. The value of G reach a maximum ~10^{-5} near the cloud base, reach a minimum of 1-2$\times$ 10^{-7} at a height of 9 km (coincident with maxima in N_i) and again increase upward. In case 3 (doubled $\bar{r}$), G is twice as large since $G \sim \bar{r}$; note that the $\bar{r}$ dependence of G results in much smaller values of G for liquid clouds (KC99b) than for ice clouds. Cases 2 and 4 both show the same values of G as in the baseline case; in case 2, the increase in IWC is compensated in (2.12) by increase in $\bar{r}$ and in case 4 G does not depend on k.

Corresponding profiles of the index p calculated from (3.2) with c_{nn} = 1 are shown in Fig. 2b. In the baseline case, the values of p are negative, from 0 to -9, in the cloud evaporation layer with $S < 0$ below 7 km. Values of p are positive, ranging from 0 to 13, in the cloud growth layer with $S > 0$. These variations in p are caused by simultaneous variations in S and G. As discussed in section 5, the values of p for this cirrus cloud are comparable to those in liquid Arctic St cloud considered in Curry (1986) and KC99b, since larger G in Ci are compensated in (5.1) by larger $\bar{r}$.

The values of p decrease by a factor of 2 with doubled k (case 4, asterisks) since $p \sim k^{-1}$; this causes an increase in relative dispersions σ_r according to (1.3) and reflects the effect of stochastic condensation as increasing turbulence broadens the spectra. The values of p decrease by a factor of 4 with doubled $\bar{r}$ (crosses) since $p \sim G^{-2}$, which is also an effect of stochastic condensation. As follows from kinetic equations (2.1) or (2.6), we can introduce the diffusion coefficient in radii-space as $k_r = c_{nn}G^2k$, so that the 3rd term on the right-hand side of (2.6) describing diffusion in radii space can be written as $k_r(\partial^2 f/\partial r^2)$. According to (2.12), $G \sim \bar{r}/q_{ls}$, thus, $k_r \sim \bar{r}^2$ for fixed q_{ls}. This feature resembles Taylor's diffusion with the diffusion coefficient $k \sim l^2$, with l being mixing length. In stochastic condensation, $\bar{r}$ is a characteristic length and plays the role of mixing length in radii space.

Shown in Fig. 3 are the slopes β_s of calculated from (4.3) in the upper layer with ice supersaturation at heights 7.5 - 8.7 km and in the lower layer at heights 4.8 - 6.0 km with $S < 0$. The common feature in both layers is substantial increase of the slopes with increasing radius, which arises from the dominance of the second term with $v(r)$ in (4.3) that tends to the limit (4.7). In the upper layer, the slopes decrease downward causing spectral broadening, which agrees with observations. This is caused by dominance of the terms with α_s, and decrease of $|\alpha_s|$ downward, toward the level with $S = 0$. In the lower layer, the values of β_{s2} are much smaller due to smaller α_s (see Fig. 1d) and increase downward. The last feature would cause an incorrect narrowing of the spectra downward, but it is overwhelmed by the effect of the negative indices p in this layer as described below.

Fig. 4 depicts size spectra $f_s(r)$ calculated with input profiles from the baseline case. The left panels (a, c) show the tails of the spectra calculated from (4.4), and the right panels (b, d) show the composite spectra (4.5) with multiplication by $r^p\Phi(r)$ and $\Phi(r)$ from (4.6). One can see that in the upper ice supersaturated layer with $p > 0$, the spectra resemble typical gamma distributions. Addition of the factor $r^p\Phi(r)$ allows extension of the spectra to the small radii region but does not cause substantial change of the spectra.

The situation is different in the lower ice subsaturated layer with $p < 0$. Without the factor $r^p\Phi(r)$, the small size region up to 100 μm in double log coordinates represents parallel straight lines with positive slopes caused by the factor r before exponent in (4.4) (recall, the solution (4.4) is typical for some previous theories of stochastic condensation with $p = 1$). With multiplication by $r^p\Phi(r)$ in (4.5), the spectra become inverse power laws up to $r \sim 40$ - 50 μm, the slopes (indices p) increase with height (i.e., with decreasing temperature); and the spectra show bimodality with secondary maxima at $r = 100$ - 150 μm (Fig. 4d). Such bimodal behavior is often observed in crystalline clouds and parameterized with superposition of the two inverse power laws or gamma distributions that correspond to the two size fractions (e.g., HP84, Mitchell et al. 1996; Platt 1997, Ryan 2000). Eq. (4.5) and Fig. 4d show that this bimodality may occur within the small-size fraction: the left branch (inverse power law) is a result of stochastic and regular condensation, while the tail is dominated by the interaction of regular condensation, turbulent and convective transport, and sedimentation. A comparison with experimental data is performed in Part 2 and shows that these calculated spectra well describe the typical features of the crystal spectra measured in cirrus clouds and addition of the large fraction may cause multi-modality.

7. Conclusions

The stochastic kinetic equation for the drops and ice crystal size spectra $f(r)$ derived in KC99a is extended here to include the accretion/aggregation processes. Under a number of assumptions typical for the cloud bulk models, analytical solutions to the kinetic equation are obtained here for the small-size fraction of the cloud droplet and crystal size spectra. The solutions obtained for the small-size fraction have the form

$$f_s(r) = c_N r^p \exp(-\beta(r) r^\lambda)\Phi(r)\,. \tag{7.1}$$

i.e., are close to generalized gamma distributions.

A general yet simple analytical expression is found for the index p, which is expressed via supersaturation, cloud integral parameters (liquid or ice water content, mean radius or number density), and a few fundamental constants. Depending on supersaturation, the index p can be positive, yielding gamma distributions, or negative, yielding inverse power laws. The positive values of p can vary in the range 0 - 12 in stratiform clouds, and can reach 30-40 for convective clouds. The range of negative p values is 0 to - 12, close to observations in liquid and crystalline clouds. The values and profiles of p provide a physical explanation of the observed spatio-temporal variations of the relative dispersions observed in various cloud types. These values of p correspond to dispersions that are smaller than in many previous theories, providing better agreement with observations than previous theoretical values that yielded spectra broader than observed. In evaporating layers with negative p, the expression (7.1) yields a bimodal spectra within small-size fraction alone, and the spectra represent a product of the exponent and the Heymsfield-Platt inverse power law.

This simple expression for the index p can be easily incorporated in bulk microphysics parameterizations instead of prescribed values for p for cloud drop and ice crystal size spectra in cloud and climate models that include supersaturation fluctuations (e.g., Morrison et al., 2005a,b; Morrison and Pinto 2005; Gettelman and Kinnison 2007) or parameterize them via subgrid velocities.

The two analytical solutions obtained here differ by the account or neglect of the condensation/deposition in the tails of the spectra, which is determined by the magnitude of sub- or supersaturation. The slopes $\beta(r)$ of the tails are simply expressed via dynamical quantities (vertical velocity, turbulent coefficient and their derivatives), and the rate of collection of the small particles by the larger precipitating particles. The slopes of the solution neglecting condensation/deposition of the larger particles do not depend on radius for negligible fall velocities and on supersaturation, and the value of $\lambda = 1$ in (7.1). The slopes of the solution including condensation/deposition of the larger particles are inversely proportional to the supersaturation and proportional at sufficiently large radii to the terminal velocity. The slopes $\beta(r)$ of the second solution depend on radius as $\beta(r) = c_\beta r^\kappa$ with $\kappa > 1$, and the tails of the spectra have the form $\exp(-c_\beta r^\lambda)$ with λ varying from 2 to 4 for various radii and regimes of fall speeds.

The range of λ in both solutions (1 - 4) encompasses the range of fixed values of λ obtained in the other theories of size spectra cited in the Introduction (2 - 3), but in contrast to these previous theories, the values of λ derived here are not fixed but depend on the physical situation.

These solutions provide physical explanations for observed dependencies of the spectra on the temperature, turbulence, liquid water or ice water content, and other cloud properties. The results are illustrated with an example of calculations for crystalline clouds. These analytical solutions can be used for parameterization of the size spectra and related quantities (e.g., optical properties, radar reflectivities) in bulk cloud and climate models and in remote sensing techniques. They can be also used for testing the accuracy of the numerical cloud models, where the numerical diffusivity can be significant. Note that despite the existence of such kinetic equations of stochastic condensation with advection and diffusion in radii space for more than four decades and the recent refinements to the stochastic condensation theory (e.g., Liu 1995; Korolev 1995; Liu and Hallett 1998; KC99a,b; Vaillancourt et al., 2002; Shaw 2003; Paoli and Shariff 2003, 2004; Tisler et al. 2005; McGraw and Liu 2006; Jeffery et al. 2007; this work), all currently employed spectral bin models account for only advection in radii space, i.e., $\partial(\dot{r}_{cond} f_s)/\partial r$ in (2.1), (2.6), and neglect the diffusion by radius, $G^2 k^{nn} \partial^2 f / \partial r^2$, and cross-derivative terms, $G^2 k^n \partial^2 f / \partial r \partial z$. The error of this approximation is unknown and can be significant because these neglected terms are responsible for the broadening of the spectra and corresponding effects on coagulation-accretion and cloud optical properties.

Analytical solutions have been presented here for liquid only and ice only size spectra. Treatment of mixed-phase clouds would require simultaneous consideration of the kinetic equations for the drop and crystal spectra with account for their interactions. The analytical solutions for the large size spectra (precipitating particles) are considered in Part 2 of this work (KC07).

Acknowledgments. This research has been supported by the Department of Energy Atmospheric Radiation Measurement Program, and NASA Modeling and Parameterization Program. The authors are grateful to three anonymous reviewers for the useful remarks that helped to improve the text. Jody Norman is thanked for help in preparing the manuscript.

Appendix A

Solution of kinetic equation of section 3 with the Kummer equation

The solutions obtained in this work are a generalization of the corresponding solutions from KC99b. The analysis of asymptotic behavior of the individual terms in (2.11) for small values of r shows that the most singular in r are the 1st, 3rd and last terms, and hence we retain in (2.11) only these terms:

$$r^2 \frac{d^2 f_s}{dr^2} + a_1 r \frac{df_s}{dr} - a_1 f_s = 0 , \tag{A.1}$$

$$a_1 = -\frac{bS}{c_{nn} k G^2} . \tag{A.2}$$

Eq. (A.1) is a linear homogeneous Euler equation of 2nd order and its solution can be obtained in the form of a power law (Landau and Lifshitz 1958):

$$f_s(r) \sim r^p . \tag{A.3}$$

Substitution of (A.3) into (A.1) yields

$$p = \frac{bS}{c_{nn} k G^2} . \tag{A.4}$$

For the larger particles in the small-size fraction, where $r < r_0$, with r_0 being the boundary between the small- and large-size fractions defined in section 2, we assume that supersaturation and diffusional growth are sufficiently small that we can eliminate in (2.11) the condensation growth terms that are proportional to r^{-1} and $\sim r^{-2}$. Then (2.11) becomes

$$c_{nn} k G^2 \frac{d^2 f_s}{dr^2} + 2 c_n k G \alpha_s \frac{df_s}{dr}$$
$$+ \left[2 c_n k G \alpha_s + \alpha_s^2 k (1 - \mu_s^2) \right] f_s = 0 , \tag{A.5}$$

where

$$\mu_s = \left[\frac{1}{\alpha_s^2 k} \left(\alpha_s (w - v) + \frac{dw}{dz} + \sigma_{col} - \frac{d\alpha_s k}{dz} \right) \right]^{1/2} . \tag{A.6}$$

We seek a solution similar to KC99b as the exponential tail of the gamma distribution:

$$f_s(r) \propto \exp(-\beta_s r) . \tag{A.7}$$

Substitution into (A.5) yields a quadratic equation for β_s

$$c_{nn} k G^2 \beta_s^2 - 2 c_n k G \alpha_s \beta_s + k \alpha_s^2 (1-\mu_s^2) = 0 , \tag{A.8}$$

which has two solutions for β_s

$$\beta_{s,1,2} = \frac{c_n k \alpha_s \mp \left(c_n^2 k^2 \alpha_s^2 - c_{nn} k^2 \alpha_s^2 (1-\mu_s^2) \right)^{1/2}}{c_{nn} k G} . \tag{A.9}$$

Hereafter in this section, the negative and positive signs relate to the 1st and 2nd solutions respectively. Eq. (A.7) represents the exponential tail of the spectrum and the slopes (A.9) are generalizations of the corresponding expression from KC99b. Physical conditions require that $\beta_{s,1,2} > 0$.

In KC99b, the details of the derivation and solution of the Kummer equation for the interpolation function Φ were omitted. Note that a similar technique is standard and widely used in solutions of the numerous problems of quantum mechanics and atomic physics (e.g., Landau and Lifshitz 1958), and could be used in cloud physics. Here, we present the details because of potential use of this technique for the bulk cloud models. It is convenient to rewrite composite spectrum (3.7), the product of (A.3) and (A.7), with auxiliary function $\eta(r)$

$$f_s(r) = \eta(r)\Phi(r) , \tag{A.10}$$

$$\eta(r) = c_{1,2} r^p \exp(-\beta_s r) . \tag{A.11}$$

First, we assume that $v(r)$ = const, then μ_s = const, and β_s = const, a correction for r-dependence of the terminal velocities can be accounted for by introducing real $v(r)$ into the final solutions. The derivatives f_s' and f_s'' are expressed as

$$f_s' = (p/r - \beta)\eta\Phi + \eta\Phi' , \tag{A.12}$$

$$f_s'' = (p/r - \beta)^2 \eta\Phi - (p/r^2)\eta\Phi + 2(p/r - \beta)\eta\Phi' + \eta\Phi'' . \tag{A.13}$$

Substitution of (A.3), (A.4) into (2.11) and deleting $\eta(r)$ in the resulting equation yields

$$G^2 k\left[\left(\frac{p}{r}-\beta\right)^2\Phi-\frac{G^2kp}{r^2}\Phi+2\left(\frac{p}{r}-\beta\right)\Phi'+\Phi''\right]$$

$$+\left(2G\alpha_s k-\frac{bS}{r}\right)\left[\left(\frac{p}{r}-\beta\right)\Phi+\Phi'\right]\left[\alpha_s^2 k(1-\mu_s^2)+\frac{bS}{r^2}\right]=0\,. \qquad \text{(A.14)}$$

Collecting now the terms with various derivatives of Φ, we obtain an equation

$$A_1\frac{d^2\Phi}{dr^2}+A_2\frac{d\Phi}{dr}+A_3\Phi=0\,, \qquad \text{(A.15)}$$

where

$$A_1=G^2k\,, \qquad \text{(A.16)}$$

$$A_2=\left(\frac{2G^2kp}{r}-2G^2k\beta_s+2G\alpha_s k-\frac{bS}{r}\right), \qquad \text{(A.17)}$$

$$A_3=\frac{G^2kp^2}{r^2}-\frac{2G^2kp\beta_s}{r}+G^2k\beta_s^2-\frac{G^2kp}{r^2}+\frac{2G\alpha_s kp}{r}-\frac{bSp}{r^2}-2G\alpha_s k\beta_s$$

$$+\frac{bS\beta_s}{r}+\alpha_s^2k(1-\mu_s^2)+\frac{bS}{r^2}\,. \qquad \text{(A.18)}$$

These coefficients are significantly simplified after substituting the expression $bS = G^2kp$ that follows from (3.2) (with c_{nn} =1) and (3.6) for β_s. First, for $\beta_{s1} = (\alpha_s/G)(1-\mu_s)$, we have

$$A_3=-\frac{2Gkp\alpha_s}{r}+\frac{2Gkp\alpha_s\mu_s}{r}+k\alpha_s^2-2k\alpha_s^2\mu_s+k\alpha_s^2\mu_s^2+\frac{2G\alpha_s kp}{r}$$

$$-2\alpha_s^2k+2\alpha_s^2k\mu_s+\frac{Gk\alpha_s p}{r}-\frac{Gk\alpha_s p\mu_s}{r}+k\alpha_s^2-\alpha_s^2k\mu_s^2\,. \qquad \text{(A.19)}$$

This equation contains 12 terms, but one can see that the following 9 terms are mutually cancelled: 1st and 6th; 4th and 8th; 3rd, 7th and 11th; 5th and 12th. The rest 3 terms yield

$$A_3=\frac{Gk\alpha_s p}{r}(1+\mu_s) \qquad \text{(A.20)}$$

The coefficient A_2 is also simplified after substitution of bS via p and β_{s1}:

$$A_2 = \frac{2G^2kp}{r} - 2G^2k\frac{\alpha_s}{G}(1-\mu_s) + 2G\alpha_s k - \frac{G^2kp}{r} = G^2k\left(\frac{p}{r} + \frac{2\alpha_s\mu_s}{G}\right). \tag{A.21}$$

Substituting these reduced A_2, A_3 into (A.15), dividing by G^2k and multiplying by r we obtain the equation for Φ with $\beta_{s,1}$

$$r\Phi'' + \left(p + \frac{2\alpha_s\mu_s}{G}r\right)\Phi' + \frac{\alpha_s p}{G}(1+\mu_s) = 0\,. \tag{A.22}$$

A solution to this equation is the confluent hypergeometric (Kummer) function (Landau and Lifshitz 1958, hereafter LL58; Gradshteyn and Ryzhik 1994, hereafter GR94)

$$\Phi(r) = c_1 F\left(\frac{p}{2\mu_s}(\mu_s+1), p; -\frac{2\alpha_s\mu_s}{G}r\right). \tag{A.23}$$

Then the full solution for f_s is

$$f_{s,1}(r) = c_1 r^p \exp\left(-\frac{\alpha_s}{G}(1-\mu_s)\right),$$

$$\times F\left(\frac{p}{2\mu_s}(\mu_s+1), p; -\frac{2\alpha_s\mu_s}{G}r\right), \tag{A.24}$$

For $\beta_{s2} = (\alpha_s/G)(1+\mu_s)$, substituting it and $bS = G^2kp$ into (A.18) for A_3, we obtain

$$A_3 = -\frac{2Gkp\alpha_s}{r} - \frac{2Gkp\alpha_s\mu_s}{r} + k\alpha_s^2 + 2k\alpha_s^2\mu_s + k\alpha_s^2\mu_s^2 + \frac{2G\alpha_s kp}{r}$$

$$-2\alpha_s^2 k - 2\alpha_s^2 k\mu_s + \frac{Gk\alpha_s p}{r} + \frac{Gk\alpha_s p\mu_s}{r} + k\alpha_s^2 - \alpha_s^2 k\mu_s^2\,. \tag{A.25}$$

Here also, the following terms are mutually cancelled: 1st and 6th; 3, 7th and 11th; 4th and 8th; 5th and 12th. The rest 3 terms yield

$$A_3 = \frac{Gk\alpha_s p}{r}(1-\mu_s)\,. \tag{A.26}$$

The coefficient A_2 in (A.17) is simplified after substitution of bS via p and β_{s2}:

$$A_2 = \frac{2G^2kp}{r} - 2G^2k\frac{\alpha_s}{G}(1+\mu_s) + 2G\alpha_s k - \frac{G^2kp}{r} = G^2k\left(\frac{p}{r} + \frac{2\alpha_s\mu_s}{G}\right) \tag{A.27}$$

Again substituting reduced A_2, A_3 into (A.15), dividing by G^2k and multiplying by r we obtain the equation for Φ with $\beta_{s,2}$

$$r\Phi'' + \left(p - \frac{2\alpha_s \mu_s}{G} r\right)\Phi' + \frac{\alpha_s p}{G}(1-\mu_s) = 0 . \tag{A.28}$$

A solution to this equation is the confluent hypergeometric function (GR94)

$$\Phi(r) = c_2 F\left(\frac{p}{2\mu_s}(\mu_s - 1), p; +\frac{2\alpha_s \mu_s}{G} r\right). \tag{A.29}$$

The full solution for f_s is

$$f_{s,2}(r) = c_2 r^p \exp\left(-\frac{\alpha_s}{G}(1+\mu_s)\right),$$

$$\times F\left(\frac{p}{2\mu_s}(\mu_s - 1), p; +\frac{2\alpha_s \mu_s}{G} r\right), \tag{A.30}$$

The properties of confluent hypergeometric functions $F(a,b;x)$, asymptotics, evaluation of the moments and normalizing constants are described in Appendix to KC99b.

Appendix B

Solution of kinetic equation of section 4 with account for the diffusional growth in the tail

It is convenient to solve Equation (B.1) by rewriting it as

$$\frac{d}{dr}\left(\frac{f_s}{r}\right) = [\xi_1 + \xi_2(r)] f_s , \tag{B.1}$$

where

$$\xi_1 = \frac{1}{bS}\left(\alpha_s^2 k + \alpha_s \frac{dk}{dz} + k\frac{d\alpha_s}{dz} - \alpha_s w - \frac{dw}{dz} - \sigma_{col}\right), \tag{B.2a}$$

$$\xi_2 = \alpha_s v(r)/bS . \tag{B.3b}$$

Introducing a new variable $\varphi_s = f_s(r)/r$, (B.1) can be rewritten as

$$\frac{d\varphi_s}{dr} = [\xi_1 + \xi_2(r)] r\varphi_s . \tag{B.4}$$

Integration from some r_1 to r yields

$$\varphi_s(r) = \varphi_s(r_1)\exp(J_{s1} + J_{s1}), \tag{B.5}$$

where

$$J_{s1} = \int_{r_1}^{r} \xi_1 r dr = \frac{(r^2 - r_1^2)\xi_1}{2}, \tag{B.6}$$

$$J_{s2} = \int_{r_1}^{r} \xi_2(r) r dr = \frac{\xi_2(r) r^2 - \xi_2(r_1) r_1^2}{B_v + 2}. \tag{B.7}$$

When evaluating J_{s2}, we assume that $v(r)$ at this size range can be approximated by the power law (2.9) with constant A_v, B_v. Substituting these integrals into (B.5), and again using $f_s = \varphi_s/r$, we obtain the solution for the larger portion of the small fraction $r < r_0$:

$$f_s(r) = \frac{r}{r_1} f_s(r_1)\exp\{-[\beta_{s2}(r) r^2 - \beta_{s2}(r_1) r_1^2\}. \tag{B.8}$$

where the slope β_{s2} is

$$\beta_{s2} = -\left(\frac{\xi_1}{2} + \frac{\xi_2}{B_v + 2}\right)$$

$$= \frac{1}{bS}\left(\frac{\alpha_s w + dw/dz + \sigma_{col} - \alpha_s^2 k - \alpha_s k' - k\alpha_s'}{2} - \frac{\alpha_s v(r)}{B_v + 2}\right), \tag{B.9}$$

and the primes denote here derivatives by z. This is the solution for the tail of the small fraction expressed via its value at $r = r_1$.

References

Ackerman, S. A., and G. L. Stephens, 1987: The absorption of solar radiation by cloud droplets: An application of anomalous diffraction theory. *J. Atmos. Sci*., **44**, 1574-1588.

Austin, P. H., M. B. Baker, A. M. Blyth, and J. B. Jensen, 1985: Small-scale variability in warm continental cumulus clouds. *J. Atmos. Sci*., **42**, 1123-1138.

Borovikov, A. M., I. P. Mazin, and A. N. Nevzorov, 1965: Some features of distribution of the large particles in clouds of various forms. *Izv. Acad. Sci. USSR, Atmos. Oceanic Phys*., **1** (3), 357-369.

Brenguier, J.-L., and L. Chaumat, 2001: Droplet spectra broadening in cumulus clouds. Part I: broadening in adiabatic cores. *J. Atmos. Sci.*, **58**, 628–641.

Buikov, M. V., 1961: Kinetics of distillation in a polydisperse fog. *Izv. Acad. Sci. USSR, Ser. Geophys*., **7**, 1058 - 1065.

_____, 1963: A method of the kinetic equations in the theory of clouds. *Proc. All-Union Meteorol. Conf*., Leningrad, **5**, 122-128.

Clark, T., 1974: A study in cloud phase parameterization using the gamma distribution. *J. Atmos. Sci.,* **31**, 142-155.

Cohard, J.-M., and J.-P. Pinty, 2000: A comprehensive two-moment warm microphysical bulk scheme. I: Description and tests. *Q. J. Roy. Meteorol. Soc*., 126, 1815-1842.

Considine, G. and J. A. Curry, 1996: A statistical model of drop size spectra for stratocumulus clouds. *Quart. J. Roy. Meteor. Soc*., **122**, 611-634.

Cotton, W. R., R. A. Anthes, 1989: *Storm and Cloud Dynamics,* Academic Press, 883 pp.

_____, G. J. Tripoli, R. M., Rauber, and E. A. Mulvihill, 1986: Numerical simulation of the effects of varying ice nucleation rates and aggregation process on orographic snowfall. *J. Climate Appl. Meteorol*., **25**, 1658-1680.

Curry, J. A., 1986: Interactions among turbulence, radiation and microphysics in Arctic stratus clouds. *J. Atmos. Sci*., **43**, 525-538.

_____, and P. J. Webster, 1999: *Thermodynamics of Atmospheres and Oceans,* Academic Press, London, 467 pp.

_____, E. E. Ebert, and G. F. Herman, 1988: Mean and turbulent structure of the summertime Arctic cloudy boundary layer. *Quart. J. Roy. Meteor. Soc*., **114**, 715-746.

Dyachenko, P. V., 1959: Experience of application of the methods of mathematical statistics to the studies of clouds and fogs microstructure. *Proc. Main Geophys. Obs*., Leningrad, **101**, 32-45.

Ferrier, B. S., 1994: A double-moment multiple-phase four-class bulk ice scheme. Part I: Description. *J. Atmos. Sci.,* **51***,* 249-280.

Fowler, L. D., D. A. Randall and S. A. Rutledge, 1996: Liquid and ice cloud microphysics in the CSU general circulation model. Part I: Model description and simulated microphysical processes. *J. Climate,* **9**, 489-529.

Ghan, S., L. Leung, R. Easter, and H. Abdul-Razzak, 1997: Prediction of cloud droplet number in a general circulation model, *J. Geophys. Res.,* **102**, 777-794.

Gettelman, A., and D. E. Kinnison, 2007: The global impact of supersaturation in a coupled chemistry-climate model. *Atmos. Chem. Phys.,* **7**, 1629-1643.

Girard, E., and J. A. Curry, 2001: Simulation of Arctic low-level clouds observed during the FIRE Arctic Clouds Experiment using a new bulk microphysics scheme. *J. Geophys. Res.,* **106,** 15139-15154.

Gradshteyn, I. S. and I. M. Ryzhik, 1994: *Table of Integrals, Series, and Products*, 5th ed., A. Jeffery, Ed., Academic Press, 1204 pp.

Hall, W. D. and H. R. Pruppacher, 1976: The survival of ice particles falling from cirrus clouds in subsaturated air. *J. Atmos. Sci*., **33**, 1995-2006.

Harrington, J. Y., M. P. Meyers, R. L. Walko, and W. R. Cotton, 1995: Parameterization of ice crystal conversion process due to vapor deposition for mesoscale models using double-moment basis functions. Part I: Basic formulation and parcel model results. *J. Atmos. Sci.,* **52***,* 4344–4366.

Herman G. F., and J. A. Curry, 1984: Observational and theoretical studies of solar radiation in Arctic stratus clouds. *J. Clim. Appl. Met*., **23**, 5-24.

Heymsfield, A. J. and C. M. R. Platt, 1984: A parameterization of the particle size spectrum of ice clouds in terms of the ambient temperature and the ice water content. *J. Atmos. Sci.,* **41**, 846-855.

Jeffery, C. A., J. M. Reisner, and M. Andrejczuk, 2007: Another look at stochastic condensation for subgrid cloud modeling: adiabatic evolution and effects. *J. Atmos. Sci.,* **64**, 3953 - 3973.

Jensen, E. J., O. B. Toon, D. L. Westphal, S. Kinne, and A. J. Heymsfield, 1994: Microphysical modeling of cirrus, 1. Comparison with 1986 FIRE IFO measurements, *J. Geophys. Res., 99*, 10421-10442.

_____, O. B. Toon, S. A. Vay, J. Ovarlez, R. May, T. P. Bui, C. H. Twohey, B. W. Gandrud, R. F. Pueschel, and U. Schumann, 2001: Prevalence of ice-supersaturated regions in the upper troposphere: implications for optically thin ice cloud formation, *J. Geophys. Res.,* 106, 17253-17266.

Kessler, E., 1969: On the distribution and continuity of water substance in atmospheric circulation. *Meteorol. Monogr.,* **10**, No.32, Amer. Meteor. Soc., 84 pp.

Khvorostyanov, V. I., and J. A. Curry, 1999a: Toward the theory of stochastic condensation in clouds. Part I: A general kinetic equation. *J. Atmos. Sci*., **56**, 3985-3996.

_____, and _____, 1999b: Toward the theory of stochastic condensation in clouds. Part II. Analytical solutions of gamma distribution type. *J. Atmos. Sci*., **56**, 3997-4013.

_____, and _____, 2002: Terminal velocities of droplets and crystals: power laws with continuous parameters over the size spectrum. *J. Atmos. Sci.,* **59,** 1872-1884.

_____, and _____, 2005. Fall velocities of hydrometeors in the atmosphere: Refinements to a continuous analytical power law. *J. Atmos. Sci.,* **62**, 4343–4357.

_____, and _____, 2008: Analytical solutions to the stochastic kinetic equation for liquid and ice particle size spectra. Part II: Large-size fraction in precipitating clouds. *J. Atmos. Sci.,* **64**, XX-XX.

_____, and K. Sassen, 1998: Cirrus cloud simulation using explicit microphysics and radiation. Part II, Microphysics, vapor and ice mass budgets, and optical and radiative properties, *J. Atmos. Sci.,* **55**, 1822-1845.

_____, and K. Sassen, 2002: Microphysical processes in cirrus and their impact on radiation, a mesoscale modeling perspective, in *"Cirrus",* Oxford University Press, Eds. D. Lynch, K. Sassen, D. Starr and G. Stephens, 397-432.

_____, J. A. Curry, J. O. Pinto, M. Shupe, B. A. Baker, and K. Sassen, 2001: Modeling with explicit spectral water and ice microphysics of a two-layer cloud system of altostratus and cirrus observed during the FIRE Arctic Clouds Experiment. *J. Geophys. Res*., *106*, 15,099-15,112.

Korolev, A. V., 1995: The influence of supersaturation fluctuations on droplet size spectra formation. *J. Atmos. Sci.,* **52**, 3620 - 3634.

Landau, L. D., and E. M. Lifshitz, 1958: *Quantum Mechanics, Non-Relativistic Theory. Volume 3 of Course of Theoretical Physics*, Addison-Wesley Publishing Company, Inc., 526p.

Lawson, R. P., B. Baker, B. Pilson, and Q. Mo, 2006: In situ observations of the microphysical properties of wave, cirrus, and anvil clouds. Part II: Cirrus clouds. *J. Atmos. Sci.,* **63**, 3186-3203.

Levin, L. M., 1954: On the size distributions functions of the cloud and rain droplets. *Dokl. Acad. Sci. USSR*, **44** (6), 1045-1049.

_____, and Y. S. Sedunov, 1966: Stochastic condensation of drops and kinetics of cloud spectrum formation. *J. Rech. Atmos*., **2**, 425-432.

Lin, Y. L., Farley, R. D. and Orville H. D., 1983: Bulk parameterization of the snow field in a cloud model. *J. Climate Appl. Meteorol.,* **22**, 1065-1092.

Liu, Y., 1995: On the generalized theory of atmospheric particles systems. *Adv. Atmos. Sci.,* **12**, 419-438.

______, Y. Laiguang, Y. Weinong, and L. Feng, 1995: On the size distribution of cloud droplets. *Atmos. Res.,* **35**, 201-216.

______, and J. Hallett, 1998: On size distribution of cloud drops growing by condensation: A new conceptual model. *J. Atmos. Sci.,* 55, 527-536.

Ludwig, F. L., and E. Robinson, 1970: Observations of aerosols and droplets in California stratus. *Tellus*, **22** (1), 78-89.

Manton, M. J., 1979: On the broadening of a droplet distribution by turbulence near cloud base: *Quart. J. Roy. Meteor. Soc*., **105**, 899-914.

Matrosov, S. Y., B. W. Orr, R. A. Kropfli, and J. B. Snider, 1994: Retrieval of vertical profiles of cirrus clouds microphysical parameters from Doppler radar and infrared radiometer measurements. *J. Appl. Meteor.,* **33**, 617-626.

McGraw, R., and Y. Liu, 2006: Brownian drift-diffusion model for evolution of droplet size distributions in turbulent clouds. *Geophys. Res. Lett.,* **33**, L03802, doi: 10.1029/2005GL023545.

Meyers, M. P., R. L. Walko, J. Y. Harrington, and W. R. Cotton, 1997: New RAMS cloud microphysics parameterization. Part II: The two-moment scheme. *Atmos. Res., 45,* 3-39.

Milbrandt, J. A., and M. K. Yau, 2005a: A multimoment microphysics parameterization. Part I: Analysis of the role of the spectral shape parameter. *J. Atmos. Sci.* **62**, 3051–3064.

______, and M. K. Yau, 2005b: A multimoment bulk microphysics parameterization. Part II: A proposed three-moment closure and scheme description, *J. Atmos. Sci.* **62**, 3065–3081.

Mitchell, D. L., 1994: A model predicting the evolution of ice particle size spectra and radiative properties of cirrus clouds. Part I: Microphysics. *J. Atmos. Sci*., **51**, 797-816.

______, S. K. Chai, Y. Liu, A. J. Heymsfield and Y. Dong, 1996: Modeling cirrus clouds. Part I: Treatment of bimodal spectra and case study analysis. *J. Atmos. Sci*., **53**, 2952-2966.

Monin, A. S., and A. M. Yaglom, 2007: *Statistical Fluid Mechanics: Mechanics of Turbulence*, v. 2, Dover, 896 pp.

Morrison, H., J. A. Curry, and V. I. Khvorostyanov, 2005a: A new double-moment microphysics parameterization for application in cloud and climate models, Part 1: Description. *J. Atmos. Sci.*, **62**, 1665-1677.

______, J. A. Curry, M. D. Shupe, and P. Zuidema, 2005b: A new double-moment microphysics scheme for application in cloud and climate models, Part 2: Single-column modeling of arctic clouds. *J. Atmos. Sci*., **62**, 1678-1693.

______, and J. Pinto 2005. Mesoscale modeling of springtime Arctic mixed-phase stratiform clouds using a new two-moment bulk microphysics scheme. *J. Atmos. Sci*., **62**, 3683-3704.

Nevzorov, A. N., 1967: Distribution of large drops in liquid stratiform clouds. *Proc. Centr. Aerolog. Observ.*, **79**, 57-69.

Noonkester, V. R., 1984: Droplet spectra observed in marine stratus cloud layers. *J. Atmos. Sci*., **41**, 829-845.

Okita, T., 1961: Size distribution of large droplets in precipitating clouds. *Tellus*, **13**, 456-467.

Paoli, R., and K. Shariff, 2003: Particle size distributions in atmospheric clouds. *Annual Res. Briefs, Center for Turbul. Res.*, NASA Ames Res. Center, 39-47.

______, and ______, 2004: Direct numerical simulation of turbulent condensation in clouds. *Annual Res. Briefs, Center for Turbul. Res.*, NASA Ames Res. Center, 305-316.

Pinto, J. O., and J. A. Curry, 1995: Atmospheric convective plumes emanating from the leads. 2. Microphysical and radiative processes. *J. Geophys. Res.,* **100**, 4633-4642.

Platt, C. M. R., 1997: A parameterization of the visible extinction coefficient in terms of the ice/water content. *J. Atmos. Sci.,* **54**, 2083-2098.

Poellot, M. R., K. A. Hilburn, W. P. Arnott, and K. Sassen, 1999: In situ observations of cirrus clouds from the 1994 ARM Southern Great Plains Intensive Observational Period. *Proc. 9th ARM Science Team Meeting*, San Antonio, Texas, March 22-26.

Pruppacher, H. R., and J. D. Klett, 1997: *Microphysics of Clouds and Precipitation*, 2nd Edition, Kluwer, 997 pp.

Quante, M., and D. O'C. Starr, 2002: Dynamical processes in cirrus clouds. In *"Cirrus",* Oxford University Press, Eds. D. Lynch, K. Sassen, D. Starr, and G. Stephens, pp. 346 - 374.

Rogers, R. R, 1979: A *Short Course in Cloud Physics*. 2nd ed., Pergamon Press, 235 pp.

Rutledge, S. A. and P. V. Hobbs, 1983: The mesoscale and microscale structure and organization of clouds and precipitation in midlatitude cyclones. VIII: A model for the "seeder-feeder" process in warm frontal rainbands. *J. Atmos. Sci.,* **40**, 1185-1206.

Ryan, B. F, 2000: A bulk parameterization of the ice particles size distribution and the optical properties in ice clouds. *J. Atmos. Sci.,* **57**, 1436-1451.

Sassen, K., and V. I. Khvorostyanov, 2007: Microphysical and radiative properties of mixed-phase altocumulus: A model evaluation of glaciation effects. *Atmos. Res.,* **84** (4), 390-398.

______, and L. Liao, 1996: Estimation of cloud content by W-band radar. *J. Appl. Meteor.,* **35**, 932-938.

______, D. O'C. Starr, and T. Uttal, 1989: Mesoscale and microscale structure of cirrus clouds: Three case studies. *J. Atmos. Sci.,* **46**, 371-396.

Sedunov, Y. S., 1974: *Physics of Drop Formation in the Atmosphere*. New York, Wiley, 234 p.

Seinfeld and Pandis 1998: *Atmospheric Chemistry and Physics*, Wiley, New York, 1326 pp.

Shaw, R. A., 2003: Particle-turbulence interactions in atmospheric clouds. *Ann. Rev. Fluid. Mech.*, **35**, 183-227.

Srivastava, R. C., 1969: Note on the theory of growth of cloud drops by condensation. *J. Atmos. Sci.*, **26**, 776-780.

Starr, D. O'C. and S. K. Cox, 1985: Cirrus clouds. Part I: A cirrus cloud model. *J. Atmos. Sci*., **42**, 2663-2681.

Tisler, P., E. Zapadinsky, and M. Kulmala, 2005: Initiation of rain by turbulence-induced condensational growth of cloud droplets. *Geophys. Res. Lett.,* **32**, L06806, doi: 10.1029/2004GL021969.

Vaillancourt, P. A, M. K. Yau, P. Bartello, W. W. Grabowski, 2002: Microscopic approach to cloud droplet growth by condensation. Part II: turbulence, clustering and condensational growth. *J. Atmos. Sci.*, **59**, 3421-3435.

Voloshchuk, V. M., and Y. S. Sedunov, 1977: A kinetic equation for the evolution of the droplet spectrum in a turbulent medium at the condensation stage of cloud development. *Sov. Meteorol. Hydrol*., **3**, 3-14.

Warner, J., 1969: The microstructure of cumulus cloud. Part I: General features of the droplet spectrum. *J. Atmos. Sci*., **26**, 1049-1059.

Young, K., 1993: *Microphysical Processes in Clouds*, Oxford University Press, 427 pp.

Figure captions

Fig. 1. Vertical profiles of the input parameters for the 4 different cases indicated in the legend and described in the text (a) ice water content, mg m^{-3}; (b) crystal concentration, L^{-1}; (c) ice supersaturation, %; (d) the parameter α_s, km^{-1}.

Fig. 2. Profiles of the parameter G (a) and (b) the index p of size spectra.

Fig. 3. Slopes β_s determined from (4.3) at various altitudes in the layers with: (a) ice supersaturation and (b) subsaturation. The heights in km are indicated in the legends.

Fig. 4. Size spectra calculated for the baseline case for the heights indicated in the legends. a) supersaturated layer using (4.4) for the tail; b) supersaturated layer using (4.5) for the composite spectra with multiplication by $r^p\Phi(r)$; c) subsaturated layer using (4.4) for the tail; d) subsaturated layer using (4.5) for the composite spectra with multiplication by $r^p\Phi(r)$. The temperature falls by ~ 8 ºC from the lower to the upper height of each layer.

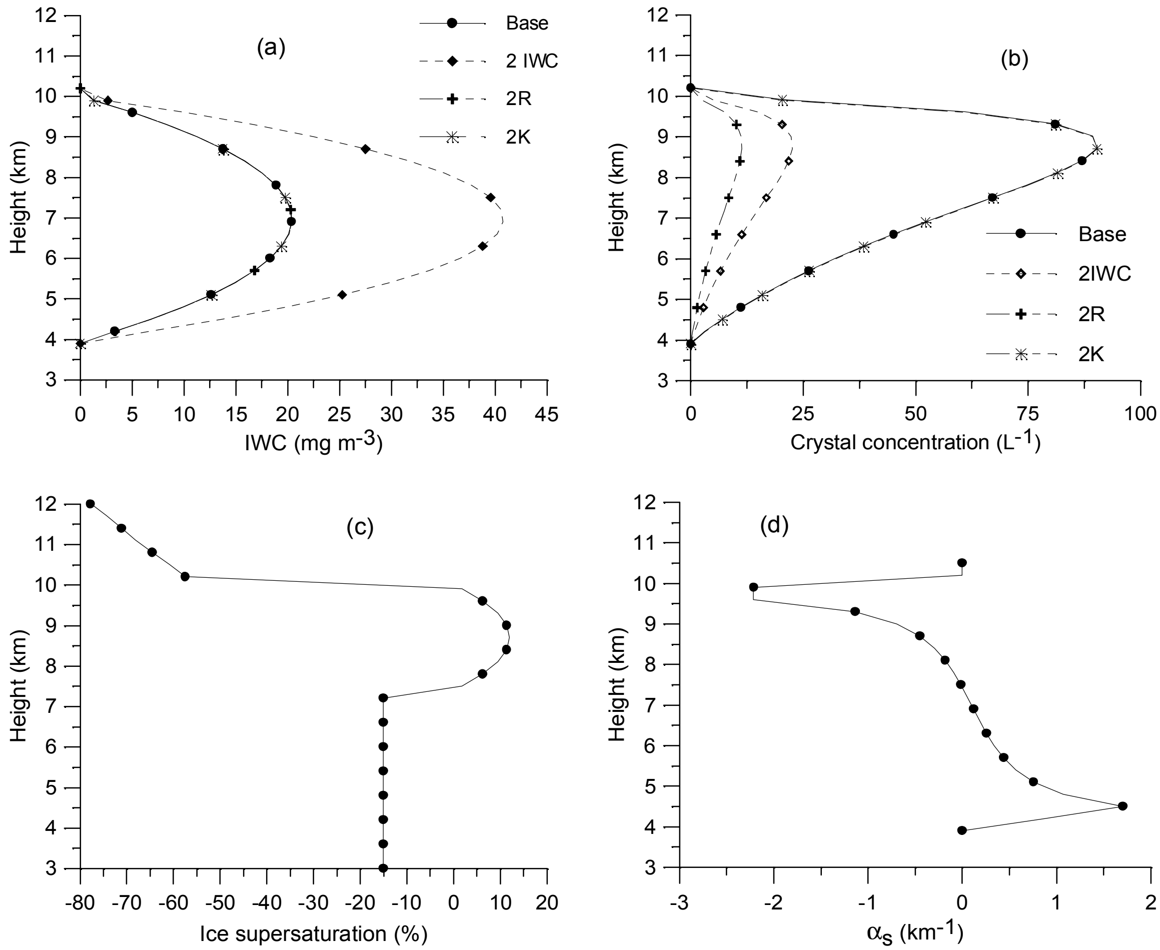
(a)
Base
2 IWC
2R
2K
Height (km)
IWC (mg m-3)
(b)
Base
2IWC
2R
2K
Height (km)
Crystal concentration (L-1)
(c)
Height (km)
Ice supersaturation (%)
(d)
Height (km)
αs (km-1)

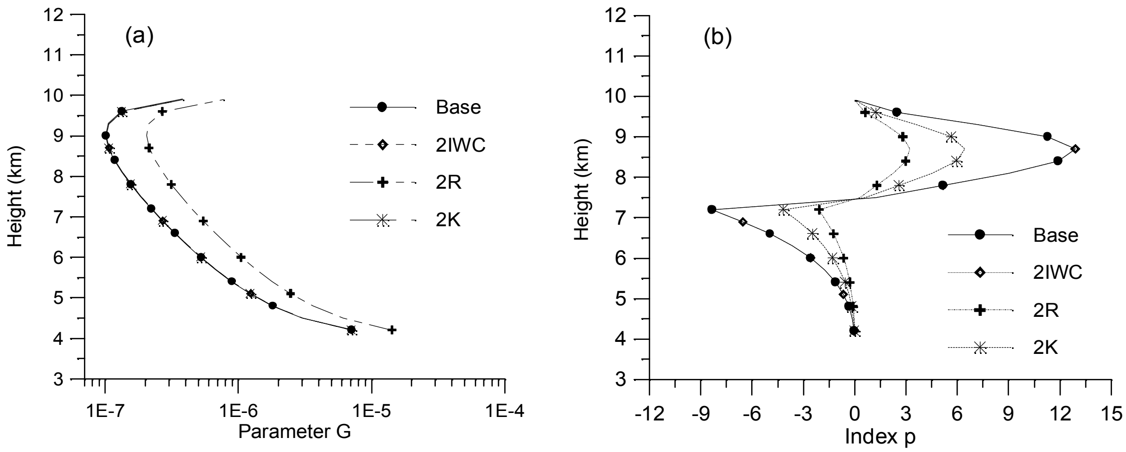

(a)
Height (km)
Parameter G
1E-7
1E-6
1E-5
1E-4
Base
2IWC
2R
2K
(b)
Height (km)
Index p
Base
2IWC
2R
2K

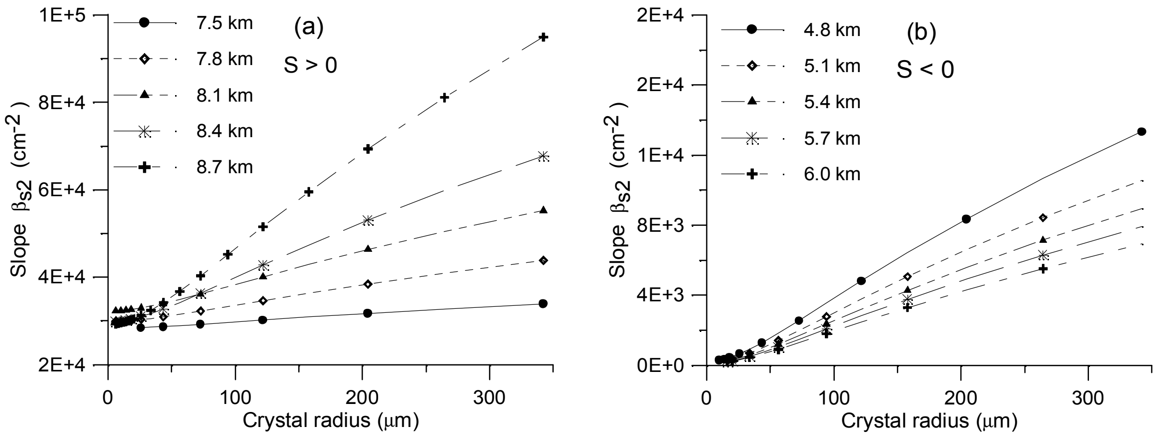

(a)
S > 0
7.5 km
7.8 km
8.1 km
8.4 km
8.7 km
Slope β_{s2} (cm^{-2})
Crystal radius (μm)
(b)
S < 0
4.8 km
5.1 km
5.4 km
5.7 km
6.0 km
Slope β_{s2} (cm^{-2})
Crystal radius (μm)

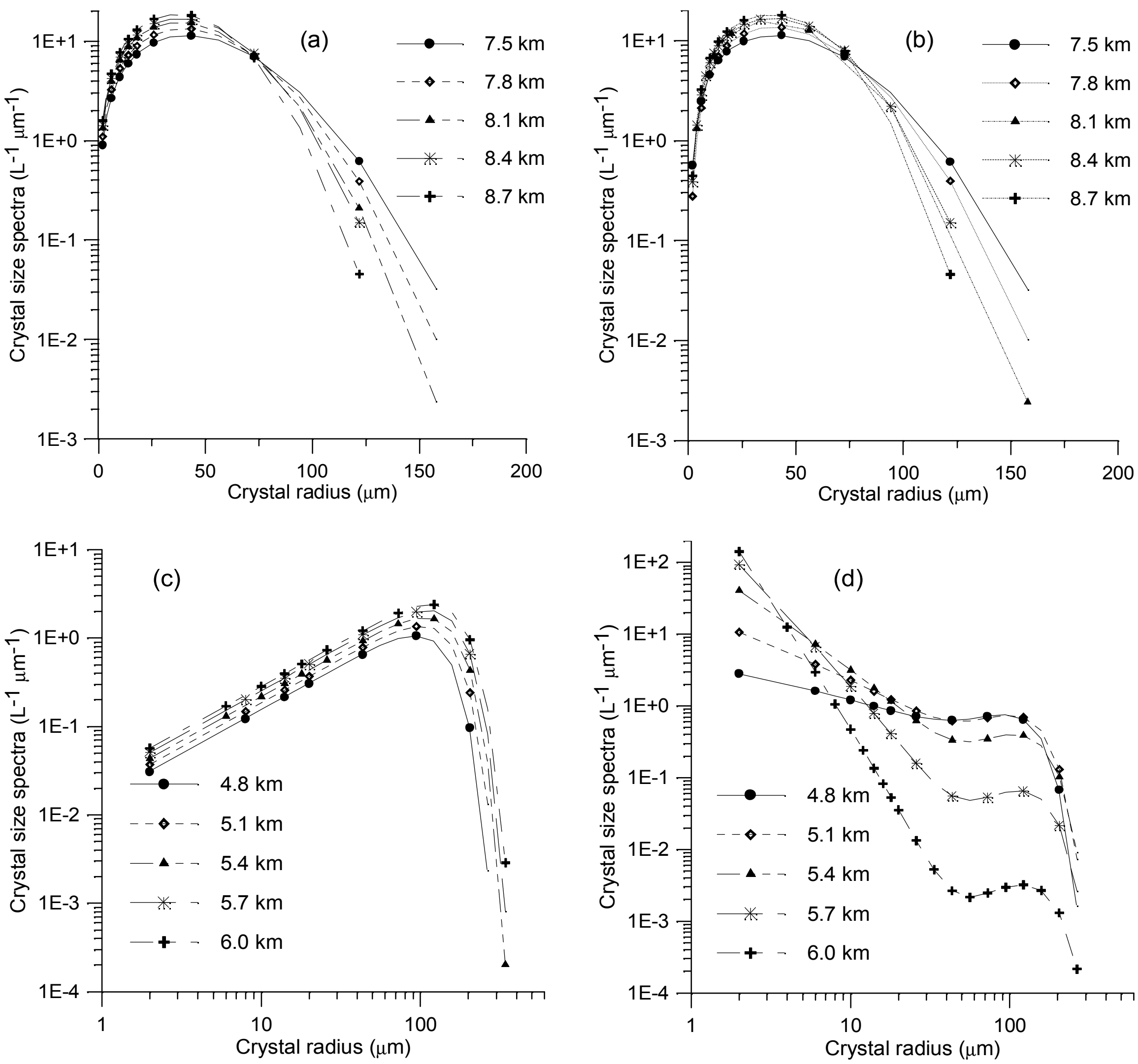
(a)
(b)
(c)
(d)
Crystal size spectra (L-1 μm-1)
Crystal radius (μm)
7.5 km
7.8 km
8.1 km
8.4 km
8.7 km
4.8 km
5.1 km
5.4 km
5.7 km
6.0 km